INSTITUTE OF PHYSICS PUBLISHING JOURNAL OF PHYSICS B: ATOMIC, MOLECULAR AND OPTICAL PHYSICS

J. Phys. B: At. Mol. Opt. Phys. **38** (2005) 1999–2013 doi:10.1088/0953-4075/38/12/014

(e, 2e) studies of H_2 in the intermediate energy regime

Andrew James Murray

Schuster Laboratory, School of Physics and Astronomy, The University of Manchester, Manchester M13 9PL, UK

E-mail: Andrew.Murray@manchester.ac.uk

Received 22 March 2005, in final form 6 May 2005
Published 6 June 2005
Online at stacks.iop.org/JPhysB/38/1999

Abstract

(e, 2e) studies have been conducted ionizing H_2 from the $X^1\Sigma_g^+$ state to the $X^2\Sigma_g^+$ H_2^+ ground state. The electron energy ranged from 10 eV through to 40 eV above the ionization threshold for experiments performed in a coplanar symmetric geometry, with both scattered and ejected electrons sharing equal energy. Results are also presented for asymmetric scattering where one of the electrons carried 80 eV energy away from the interaction in a forward direction at an angle of 35° to the incident electron beam. These experiments were performed to test the hypothesis that the two nuclei in the molecule act as a 'double scattering' centre, with the possibility of producing Young's double-slit-type interference in the resulting differential cross section. New features are found in the ionization cross section for H_2 in a coplanar symmetric geometry; however it is unclear at present if these are due to Young's double-slit interference.

1. Introduction

There has been considerable interest recently in the possibility that ionization from simple diatomic molecules may produce 'interference' effects in the ionization differential cross section (DCS) due to the localized nature of the two scattering centres in the molecule [1, 2]. These effects have been likened to Young's double-slit interference in light. Such interference effects were first predicted by Cohen and Fano for double photo-ionization [3], and evidence of this effect has been presented for ionization of molecules by ion impact [4–7]. At present, no definitive reports of these phenomena have been reported in the literature for either photo-ionization or ionization by electron impact, although Takahashi and co-workers recently reported evidence of double scattering effects from high energy electron impact ionization of hydrogen molecules fixed in space [8].

There have been several theoretical treatments indicating that this type of interaction should occur [1, 2], and so it was decided to investigate whether this could be observed

for electron impact ionization of H_2 in both a symmetric coplanar geometry and an asymmetric coplanar geometry at incident energies less than 100 eV. This energy region was chosen as it falls within the range that can be accessed using the computer controlled and computer optimized (e, 2e) spectrometer at Manchester [9]. Further work is also being carried out by Lohmann and co-workers at higher energies [10], and so a comprehensive set of evidence is expected to be produced over a wide range of energies in the near future.

An important difference between the results of Takahashi and co-workers [8] and those presented here is that the orientation of the H_2 molecules is not known in the present studies. Hence any theoretical analysis of the ionizing collision must integrate over all possible directions of the molecules with respect to the scattering geometry. There is theoretical evidence [1, 2] that this integration should still produce identifiable effects due to the two scattering centres, although the interference will be less pronounced.

An advantage of studying H_2 is that it is the simplest of all neutral molecules. The initial target state of H_2 can be defined with high precision prior to the interaction using variational principles [11], and the potential energy curve and energy levels of the resulting H_2^+ ion following the collision can be solved exactly within the Born–Oppenheimer approximation using elliptical coordinates. Hence ionization of H_2 requires minimal approximations to be made in the wavefunctions used in theoretical treatments of the scattering and ionization process. In the present studies, the temperature of the molecular beam is $\sim$300 K, and so to a high degree of probability the molecules are all in the $v = 0$ vibrational ground state. In addition, the H_2 molecules reside with a probability of greater than 95% in the $J = 0$ to $J = 3$ rotational states, with the $J = 1$ state being the highest populated at 45%. Any theoretical treatment must also therefore consider the ensemble of rotational states present in the molecular beam.

Theoretical analysis using a two-scattering centre distorted wave impulse approximation (DWIA) has also been carried out recently for ionization of N_2 [2], and the results have been compared to the experimental data produced by the Manchester and Paris groups [12, 13]. From these calculations, no net interference was predicted for a coplanar symmetric geometry from N_2 averaged over all orientations of the target. These authors *do* predict that Young's double-slit-type interference should be seen for asymmetric coplanar geometries, and the (e, 2e) spectrometer in Manchester is currently being modified to test these predictions.

In this paper experimental results are presented for ionization of H_2 in both a coplanar *symmetric* geometry, where the incident electron energy ranged from 25.3 eV through to 55.3 eV, together with results from ionization of H_2 in a coplanar *asymmetric* geometry, where the forward scattered electron carried 80 eV of energy away from the reaction at a scattering angle of 35°. The results are compared to the calculations of Stia *et al* [1], which relates the molecular cross section to that from atomic hydrogen. In both symmetric and asymmetric geometries, no clear evidence of Young's double-slit-type interference is observed; however, new features are found in the coplanar symmetric geometry that cannot be explained using the considerations usually applied to atomic targets at these energies.

In section 2 the experimental apparatus used to collect these results is detailed, together with methods used to calibrate the energy scale of the reaction. Section 3.1 details the results taken in a coplanar symmetric geometry, and section 3.2 presents the results taken in an asymmetric geometry. These are compared with the theoretical treatment of Stia and co-workers [1] in section 4 to estimate the atomic hydrogen cross section, assuming that their analysis is applicable at these energies. Finally, section 5 summarizes the results which have been obtained and draws conclusions from this analysis.

2. The experimental apparatus

2.1. The Manchester (e, 2e) spectrometer and associated scattering geometry

The (e, 2e) spectrometer at Manchester was first commissioned in 1990 [9], and since that time has been used to collect extensive experimental data for ionization of both atomic and molecular targets at low incident energies over a wide range of scattering geometries. These targets include He [14–17], Ar [18], Ne [19], Ca [20], K [21], Mg [21], Na [21], N_2 [12], CO_2 [22] and now H_2. The spectrometer was designed to measure ionization at low to intermediate energies ranging from threshold through to 300 eV incident energy, since it is in this region that the ionization cross section is largest. In this energy region the interaction leading to ionization is most complex, tolerates few approximations in theoretical models and so provides the most demanding tests of current models.

The experimental apparatus at Manchester can also be configured in a non-coplanar geometry, the electron gun being able to rotate from a coplanar geometry through to the perpendicular plane. A full three-dimensional ionization cross section is then determined, and a comprehensive set of 3D data has been published for helium [15], neon [19] and argon [18].

Unique to this (e, 2e) spectrometer are the sophisticated computer control systems which optimize and control the spectrometer throughout data collection [9]. The success of the control software and hardware has been proven since commissioning, the spectrometer having operated almost continuously since that time. The software monitors and controls the voltages on all electrostatic lens elements within the electron gun and analysers, optimizing the tuning of these lenses during operation. The electron gun is adjusted to produce an electron beam with zero beam angle and a pencil angle of 2° for energies from $\sim$10 eV through to 300 eV, with beam current up to 10 μA at higher energies. Both the current from the gun and fluorescence from interaction of the electron beam with the target are optimized using software based on a simplex routine [23]. The analysers are also optimized by adjusting their input lens voltages to maximize the yield of electrons detected by a channel electron multiplier following selection by hemispherical energy selectors. All voltages and signals from the spectrometer are continuously monitored throughout data accumulation using analogue-to-digital converters and high speed counting electronics.

In the experiments detailed here, a coplanar geometry was chosen as shown in figure 1. For coplanar *symmetric* experiments, the incident electron beam was selected to produce a current of 100 nA for an energy of 25.3 eV (10 eV above the ionization potential of H_2). The excess energy available from the interaction was shared equally by both analysers. The incident beam current was increased to 500 nA at an energy of 55.3 eV (40 eV above the ionization potential of H_2, again shared equally by both analysers). For experiments using an *asymmetric* geometry, the beam current was reduced to 290 nA at an energy of 100.3 eV. One analyser was then fixed at an angle $\theta_a = 35^\circ$ and adjusted to detect electrons at 80 eV energy. The second analyser was rotated around the scattering region and detected electrons with an energy of 5 eV.

The beam current was varied for experiments at different energies so that the scattered electron count rates measured by the analysers remained below 30 kHz. This rate had been determined previously to be the maximum acceptable to ensure effects due to pileup in the electron detectors and associated electronics are eliminated. Since the probability of scattering at lower energies was observed to increase when compared to scattering at higher energies, the spectrometer was operated at lower incident beam currents for lower energies, to ensure the count rates remained acceptable.

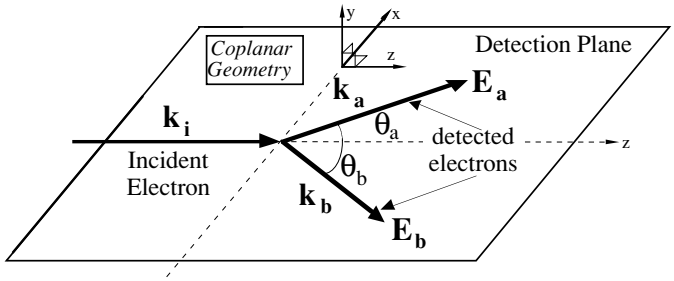

Figure 1. The coplanar geometry used in these experiments. The incident electron travels along the z-axis, and the electrons from the ionization process are detected in the xz-plane. The polar angles of the outgoing electrons are given by (θ_a, $\phi_a = 0$) and (θ_b, $\phi_b = \pi$), the electrons carrying momentum $\mathbf{k_a}$ and $\mathbf{k_b}$ respectively away from the interaction. For symmetric experiments, $\theta_a = \theta_b = \theta$, and $|\mathbf{k_a}| = |\mathbf{k_b}|$. For asymmetric geometries, $|\mathbf{k_a}| \gg |\mathbf{k_b}|$, $\theta_a = 35^\circ$ and θ_b is varied.

The molecular beam density effusing into the interaction region was kept constant throughout data accumulation, as determined by the pressure inside the vacuum chamber which was continually monitored by the control systems. The background pressure inside the vacuum chamber was measured to be $\sim 4 \times 10^{-8}$ Torr in the absence of the molecular beam using a Varian UHV ionization gauge [24]. During operation, a needle valve was used to admit hydrogen gas from a gas bottle to the chamber through an internal hypodermic needle of inner diameter 1 mm which was located 6 mm from the interaction region. The hypodermic needle pointed at an angle of 45° to the plane of the analysers and gun so as not to interfere with their positioning. The needle valve was slowly opened until the vacuum chamber pressure increased to 2.5×10^{-5} Torr, this pressure being maintained throughout data collection.

Since the operating parameters of the spectrometer were altered at each incident energy, it was not possible to place the data on a relative scale. Hence the results presented in this paper have been normalized to unity at a scattering angle of 45° for each set of data that were taken. The measured coincidence count rates ranged from ~2.5 Hz to ~0.01 Hz under these operating conditions.

2.2. Determination of the energy and associated vibrational ionic states

To establish the energy of the incident electron beam, elastic scattering measurements were taken from helium to determine the position of the elastic resonance at 19.334 eV [25]. This resonance can easily be observed by setting the analysers to monitor elastic scattering, then scanning the analyser residual energy simultaneously with that of the electron gun. A difference in energy of 1.54 V was found between the potential applied to the gun filament and that of the electron beam as shown in figure 2, this difference being due to contact potentials within the spectrometer and the work function of the filament. The beam current used in these elastic studies was 10 nA, with a vacuum chamber pressure of 1×10^{-6} Torr. The analyser was set to $\theta = 45^\circ$ for these measurements.

Once the correct energy of the electron beam was determined, the linearity of the residual energy for each analyser was established by measuring elastic and inelastic energy loss spectra from helium at various incident energies. From these spectra it was found that each analyser had a slightly different resolution due to small variations in the defining apertures within the hemispherical energy analysers. These differences were only ~50 meV, which was insignificant compared to the overall resolution of the spectrometer.

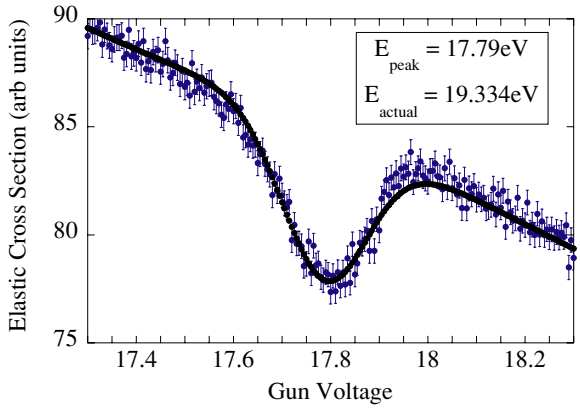

Figure 2. The elastic resonance in helium at 19.334 eV, measured at a scattering angle of 45°. The measured energy of the resonance is 17.79 eV, indicating that an offset of 1.54 V is present in the electron gun.

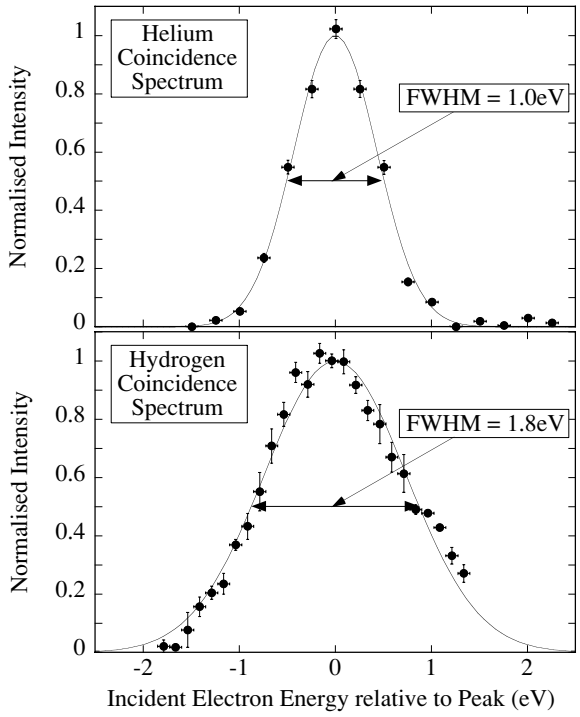

Figure 3. Relative coincidence energy spectra for He and H_2 as a function of incident energy, showing the increased width of the H_2 spectrum due to excitation of $v' = 0$ to $v' = 6$ ionic states.

The final check on energy was made by setting the analysers to detect electrons of a given energy, then scanning the incident electron beam energy through the region where an (e, 2e) coincidence signal could be measured from the target. By monitoring this coincidence signal as a function of energy for both helium and H_2, the coincidence energy width was obtained. Figure 3 shows the result of this analysis, where the relative energy of the coincidence peak

Table 1. Parameters required to derive the eigenvalues E_v and eigenfunctions $\psi_v(R)$ from the solution of Schrödinger's equation with a Morse potential.

Molecule	R_0 (Å)	D_0 (eV)	$\hbar\omega_0$ (eV)	D_e (eV)	α (Å^{-1})	x_e
H_2	0.742	4.48	0.545	4.75	1.939	0.029
H_2^+	1.06	2.65	0.284	2.79	1.319	0.025

has been set to zero for comparison. It is seen that the full width at half maximum of the coincidence spectrum for helium was ±500 meV. By contrast, the result from H_2 was significantly wider at ±900 meV.

The coincidence spectrum from helium provides a good indication of the overall energy resolution of the spectrometer, which is due to the combined resolution of the incident electron beam and that of the analysers. The electron source used in the experiment is an unselected gun whose energy width depends principally on the temperature of the filament. This width was estimated to be around ±350 meV in experiments which measure energy loss spectra from excitation of helium. The resolution of the analysers is estimated to be ±250 meV from the size of the defining apertures and pass energy of the hemispherical analysers. The combination of both the resolution of the gun and the analysers produces a width which is consistent with the overall results seen in figure 3.

Since the velocity of the helium and H_2 beams are similar, the significantly wider peak found for ionization of H_2 must therefore be due to the internal structure of the molecule. The potential energy curves for H_2 and H_2^+ can be derived from the Morse potential, where

$$V(R) = D_e[\mathrm{e}^{-2\alpha(R-R_0)} - 2\,\mathrm{e}^{-\alpha(R-R_0)}] \tag{1}$$

D_e is the minimum in the potential curve, α is a constant which depends on the restoring force binding the nuclei together and R is the inter-nuclear distance with $V(R = R_0)$ a minimum. The zero point energy D_0 is related to D_e through the relationship

$$D_e = D_0 + \tfrac{1}{2}\hbar\omega_0 \tag{2}$$

where ω_0 is approximately the angular frequency of vibration of the $v = 0$ state. The eigenvalues of the Morse potential are given by

$$E_v = \hbar\omega_0\left[\left(v + \tfrac{1}{2}\right) - x_e\left(v + \tfrac{1}{2}\right)^2\right] \tag{3}$$

where x_e is the anharmonic vibrational constant as given in table 1. The eigenfunctions using a Morse potential are given by [26]

$$\psi_v(R) = A_v\,\mathrm{e}^{-\alpha\lambda(R-R_0)}\exp\left(-\frac{\mathrm{e}^{-\alpha(R-R_0)}}{2x_e}\right)\sum_{k=0}^{v} c_k\,\mathrm{e}^{-\alpha k(R-R_0)} \tag{4}$$

where A_v is a normalization constant, $\lambda = \frac{1}{2x_e} - \left(v + \frac{1}{2}\right)$, $c_0 = 1$ and the constants c_k can be derived from the recursive formula

$$c_{k+1} = \frac{c_k}{x_e}\left[\frac{(k - v)}{(k + 1)(k + 1/x_e - 2v)}\right]. \tag{5}$$

The normalization constants A_v are obtained by calculating the appropriate integral

$$\int_{R=0}^{\infty} \psi_v^2(R)\,\mathrm{d}R = 1. \tag{6}$$

The values of the parameters in the Morse potential for both H_2 and H_2^+ are given in table 1.

Table 2. Probability of excitation $P_{v=0,v'}$ together with the associated eigen-energies of the v' ionic states excited by electron impact, for $v' = 0$ to 6. The ionization potential IP = 15.3 eV.

v'	0	1	2	3	4	5	6
$P_{v=0,v'}$	9.6%	18.2%	20.2%	17.3%	12.8%	8.6%	5.4%
$E_{v=0,v'} - \mathrm{IP}$	0 eV	0.27 eV	0.53 eV	0.77 eV	0.99 eV	1.20 eV	1.55 eV

Since ionization occurs very rapidly compared to the vibrational and rotational motion of the molecule, the Franck–Condon principle is used to establish the vibrational energy levels of the H_2^+ ion following electron impact. As the molecule remains effectively stationary during the collision, it is appropriate to map the ground $v = 0$ state of the H_2 molecule directly onto the H_2^+ vibrational states through a vertical transition (i.e. R remains unchanged).

To calculate the probability of excitation of each H_2^+ vibrational state, the Franck–Condon overlap integral is calculated between the $v = 0$ state of H_2 and the v' states of H_2^+. The probability of excitation $P_{v=0,v'}$ is then given by

$$P_{v=0,v'} = \left(\int_{R=0}^{\infty} \psi_{v=0}(R) \psi_{v'}(R) \, \mathrm{d}R \right)^2 \tag{7}$$

where the eigenfunctions are derived from equation (4). Table 2 lists the value of $P_{v=0,v'}$ for the first seven vibrational states of H_2^+, together with the relative energies of the transitions.

From table 2 it can be seen that there is significant probability of exciting ionic states $v' = 0$ to $v' = 6$ from the H_2 $v = 0$ ground state, with a range of energies up to 1.55 eV above the ionization potential of 15.3 eV. Hence the coincidence spectral width from ionization of H_2 will be comprised of the spectrometer width as measured from helium ($\sigma_{\mathrm{He}} = \pm 500$ meV) convoluted with the energy spread due to excitation of different v' ionic states ($\sigma_{H_2} \sim \pm 750$ meV). Since these are independent quantities, the total width of the H_2 coincidence peak can be estimated by taking the square root of the variances

$$\sigma_{\mathrm{coinc}} = \left(\sigma_{\mathrm{He}}^2 + \sigma_{H_2}^2 \right)^{1/2} \approx \pm 0.90 \text{ eV}. \tag{8}$$

This is in good agreement with the actual width estimated in figure 3, indicating that all ionic states from $v' = 0$ to $v' = 6$ are probably excited. Hence it is necessary for theoretical models of the ionization process to include summation over these ionic vibrational states to allow comparison with the experimental results detailed in this paper.

3. Experimental results

3.1. Coplanar symmetric geometry

Experiments were carried out in the coplanar symmetric geometry ($\theta_a = \theta_b = \theta$, $E_a = E_b$) for incident energies 10 eV, 15 eV, 20 eV, 30 eV and 40 eV above the peak ionization potential. The range of angles which could be accessed by the spectrometer ranged from $\theta = 35^\circ$ through to $\theta = 125^\circ$. The forward angles were constrained due to the Faraday cup which collected excess electrons from the electron beam, the backward scattering angles being limited by the presence of the electron gun. The analysers were advanced from $\theta = 35^\circ$ around the detection plane every 5° until an angle $\theta = 65^\circ$ was reached. Between $\theta = 65^\circ$ and $\theta = 100^\circ$ the increment in angle was reduced to 2.5° so that an unusual feature observed in the measured cross section could be detailed. From $\theta = 100^\circ$ to $\theta = 125^\circ$, the angles were again incremented by 5°.

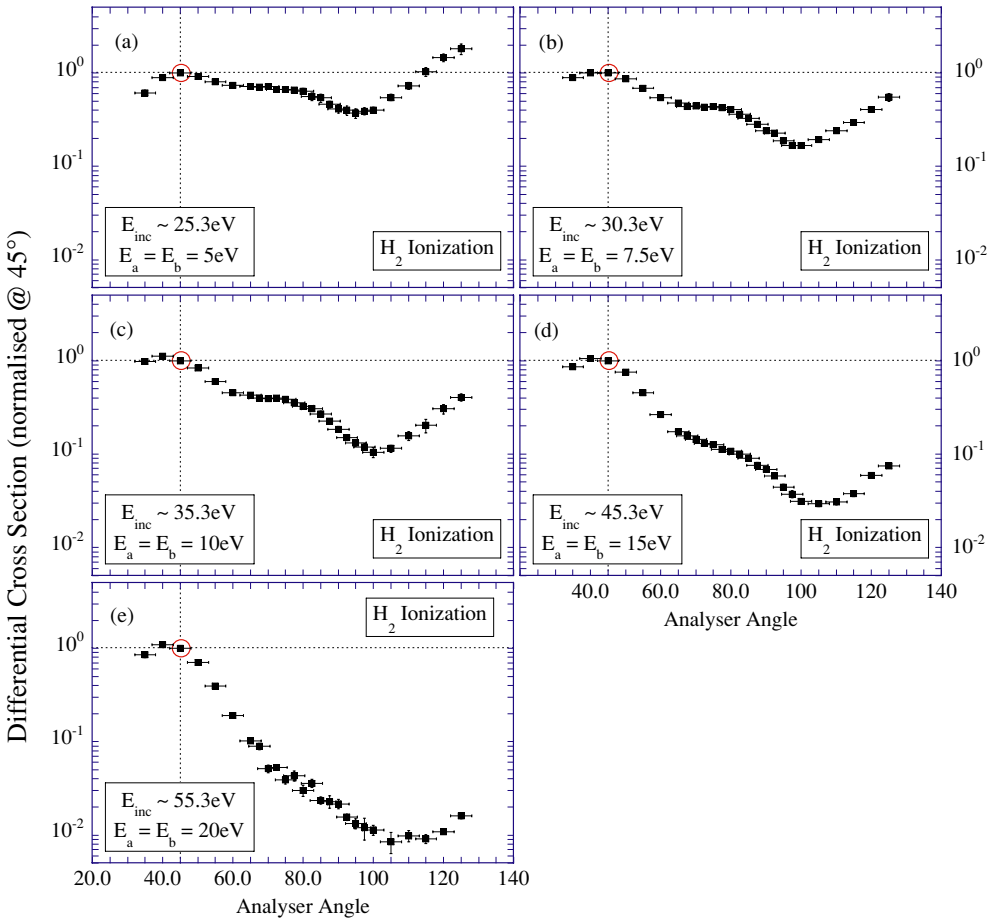

Figure 4. Experimental results for ionization of H_2 in a coplanar symmetric geometry for excess energies from (a) 10 eV to (e) 40 eV. The results are normalized at $\theta = 45^\circ$. Horizontal error bars indicate the angular acceptance of the spectrometer. For details, see text.

Results were accumulated by initially allowing the computer optimization system to tune the electron gun onto the Faraday cup signal, after which the analysers were rotated to their starting angle of $\theta = 35^\circ$. The analyser electrostatic lens elements were then computer optimized by maximizing onto the signal detected from interaction of the electron beam with the H_2 gas beam. The coincidence signal was then accumulated for a time between 1000 s and 5000 s, before the computer system moved the analyser to a new angle (in this case $\theta = 40^\circ$). The analysers were again optimized to detect electrons, and coincidence signal accumulated. This procedure was repeated until the analysers had swept through the complete angular range from $\theta = 35^\circ$ to $\theta = 125^\circ$, at which time the electron gun was re-optimized (to allow for any small drifts in the spectrometer tuning). The routine of moving the analysers and collecting coincidence signal then re-commenced, this time with the analysers moving in the opposite direction from $\theta = 125^\circ$ to $\theta = 35^\circ$. The analysers repeatedly swept around the detection plane to accumulate the coincidence data.

Figures 4(a)–(e) show the results which were obtained, normalized to unity at $\theta = 45^\circ$ as discussed above. At each incident energy the analysers were set to equal energies, and

a coincidence spectrum as a function of incident energy was measured. The electron gun was then set to the peak of the coincidence signal, and data collection commenced. Regular checks were made on the peak in the coincidence energy spectrum to eliminate any drifts in the spectrometer.

Figure 4(a) shows the results for an excess energy of 10 eV. Of particular note here is the relative magnitude of the forward scattering peak ($\theta \sim 45^\circ$) compared to the coincidence signal obtained in the backward scattering direction ($\theta \sim 125^\circ$). The signal obtained at $\theta = 125^\circ$ is 1.8 ± 0.2 greater than the magnitude at $\theta = 45^\circ$, indicating that the probability of ionization in the backward direction exceeds that for forward scattering. For ionization of atoms, the forward 'binary' peak is considered to be due to a single collision between the incident electron and one of the valence electrons, leading to a mutual scattering angle $2\theta \sim 90^\circ$ as is observed here.

By contrast, signal in the backward direction can only occur due to multiple scattering, where ionization includes the ionic core. Signal may result from the incident electron elastically scattering through 180°, followed by a binary collision between the elastically scattered electron and a valence electron. Other multiple scattering processes can also occur which result in ionization in the backward direction. In these cases, the 'recoil' peak of the backward signal is expected to occur at $\theta \sim 135^\circ$, which is beyond that which can be measured with the spectrometer. There is, however, clear evidence that the peak seen in figure 4(a) is at an angle greater than $\theta = 125^\circ$.

As the incident energy increases, the probability of scattering in the backward direction decreases relative to scattering in the forward direction. At 15 eV excess energy (figure 4(b)) the signal ratio between $\theta = 45^\circ$ and $\theta = 125^\circ$ has decreased to 0.55 ± 0.05, whereas at excess energies of 20 eV, 30 eV and 40 eV, this ratio smoothly decreases until it reaches a ratio of 0.016 ± 0.002 at 40 eV excess energy (figure 4(e)). At this energy, there is very little evidence of ionization producing signal in the backward direction.

An unusual feature in these results is the distinct feature seen at scattering angles around $\theta \sim 75^\circ$. This type of structure is not observed in ionization of atomic targets such as helium, nor does it appear in ionization of N_2, which is the only other diatomic target to have been studied at these low energies [12]. The cross section around this region was therefore measured in detail, with the analysers being incremented every 2.5° from $\theta = 65^\circ$ to $\theta = 100^\circ$ as shown. The feature appears most distinct around 15 eV to 20 eV excess energy, and is clearly visible for all energies apart from at 40 eV excess energy, where only a remnant of the feature is seen. The structure smoothly varies with scattering angle, with no evidence of sub-structure being present (within the $\sim 5^\circ$ angular resolution of the spectrometer). The minimum in the ionization cross section is seen to occur at a scattering angle $\theta \sim 105^\circ$ for all energies.

To contrast these H_2 results with those obtained from helium, figure 5 shows equivalent helium data for a coplanar symmetric geometry with excess energies ranging from 10 eV through to 40 eV, again normalized at $\theta = 45^\circ$. No results were obtained for helium at an excess energy of 15 eV.

The ionization cross section in helium is seen to smoothly vary with energy, in a similar way to H_2. By contrast, the recoil peak in helium is distinctly stronger than in H_2 at the same excess energy, and is observed to peak at $\theta \sim 115^\circ$. The helium data show a two-peak structure at all energies with distinct binary and recoil peaks. By contrast with H_2 which shows structure at $\theta \sim 75^\circ$, the cross section for helium is a *minimum* at this angle.

Table 3 quantifies these results for H_2 and He at each energy, showing the relative cross section at a scattering angle of $\theta = 75^\circ$ and at the observed peak in the backward direction ($\theta = 125^\circ$ for H_2, $\theta \sim 115^\circ$ for He). The minimum in the H_2 cross section at $\theta \sim 105^\circ$ is also shown to contrast with that observed in helium at $\theta \sim 75^\circ$.

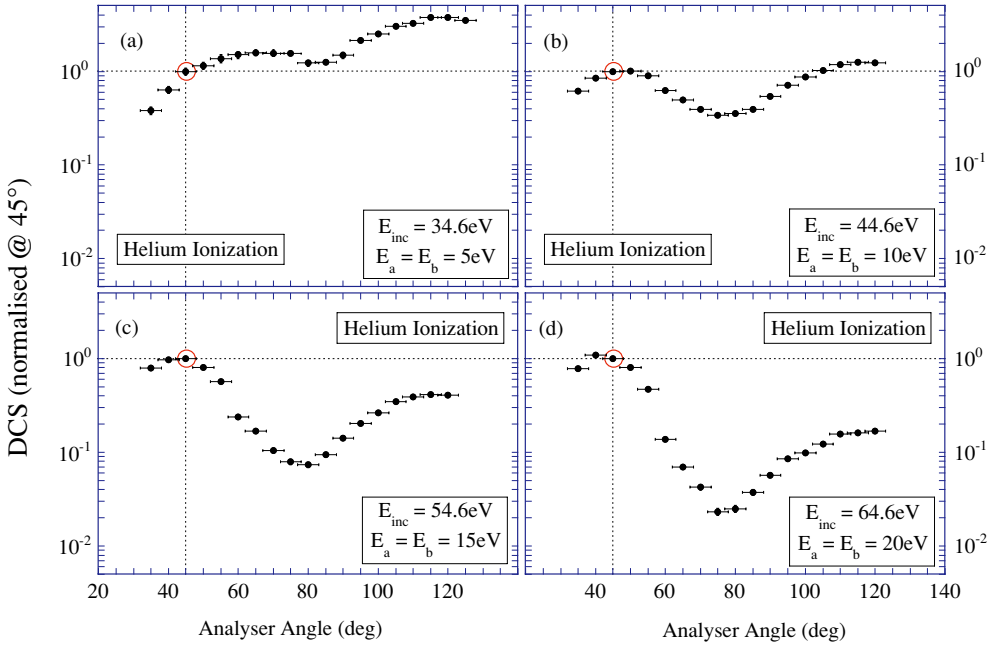

Figure 5. Comparative experimental results for ionization of He in a coplanar symmetric geometry for excess energies from (a) 10 eV to (d) 40 eV. The results are again normalized at $\theta = 45^\circ$.

Table 3. Ionization cross sections for H_2 and He as a function of excess energy, relative to the normalized cross section at $\theta = 45^\circ$. The minimum in the cross section for He appears at $\theta \sim 75^\circ$ whereas for H_2 the minimum is at $\theta \sim 105^\circ$. The recoil peak occurs at $\theta \sim 115^\circ$ in He, whereas the recoil maximum observed in H_2 is at $\theta = 125^\circ$. The relative cross section for the feature observed in H_2 at $\theta \sim 75^\circ$ is also given.

	$E_{a,b} = 5$ eV	$E_{a,b} = 7.5$ eV	$E_{a,b} = 10$ eV	$E_{a,b} = 15$ eV	$E_{a,b} = 20$ eV
$\theta = 75^\circ$ (H_2)	0.67 ± 0.04	0.44 ± 0.02	0.39 ± 0.02	0.13 ± 0.01	0.04 ± 0.01
$\theta = 75^\circ$ (He)	1.54 ± 0.06	–	0.33 ± 0.01	0.08 ± 0.01	0.023 ± 0.005
$\theta = 105^\circ$ (H_2)	0.55 ± 0.04	0.19 ± 0.01	0.11 ± 0.01	0.029 ± 0.002	0.008 ± 0.002
$\theta = 125^\circ$ (H_2)	1.81 ± 0.23	0.55 ± 0.05	0.40 ± 0.04	0.075 ± 0.004	0.016 ± 0.002
$\theta = 115^\circ$ (He)	3.77 ± 0.12	–	1.26 ± 0.02	0.41 ± 0.01	0.16 ± 0.01

Since the charged sub-atomic particles constituting H_2 and helium are identical (two electrons and two protons), it might be expected that the DCS measured from these targets would be similar. Differences between the cross sections can then be attributed to the distributed charge density found in the diatomic molecule H_2 compared to the atomic target. Helium consists of a single nucleus of charge $q = +2$ surrounded by two valence electrons which reside in the $1s^2\,{}^1S_0$ ground state prior to the collision. The nucleus can therefore, to a good approximation, be considered as a point charge at the centre of the atom. By contrast, in the $v = 0$ $X^1\Sigma_g$ ground state of H_2, the protons reside a distance $R \sim 0.742$ Å apart, with the valence electrons distributing around the nuclei so as to shield the protons from each other and stabilize the molecule against dissociation.

At large distances from both helium and H_2, the incident electrons are therefore influenced by a charge distribution which is identical for both targets. Following ionization, again at

large distances from the interaction region, the outgoing electrons will also 'see' an equivalent charge distribution from both He^+ and H_2^+ ions. The contrast between the DCS results shown in figures 4 and 5 must therefore be due to interaction of the electrons with the target in the region where differences in the charge distribution of He and H_2 become important. It is this close interaction that must be producing the new structure at $\theta \sim 75^\circ$, which moves the minimum in the cross section to $\theta \sim 105^\circ$ for H_2 compared to $\theta \sim 75^\circ$ for helium, and which produces the differences in the relative ionization cross sections for the binary and recoil peaks.

It should finally be noted that peaks around $\theta \sim 75$–90° *do* occur for atomic targets when the outgoing electron energy is small (typically less than 2 eV). These peaks are due to post-collisional interactions between outgoing electrons which have equal energy, the Coulomb interaction causing the electrons to move towards a relative asymptotic angle $2\theta = 180^\circ$. Such peaks have been observed in helium at low energies [27]; however they cannot be the cause of the feature at $\theta \sim 75^\circ$ which is seen in H_2, since this is observed at much higher excess energies.

3.2. Coplanar asymmetric geometry

Since the experimental results in a coplanar symmetric geometry are quite different to that for atomic targets, it was decided to also study the collision in an *asymmetric* geometry, where the theoretical predictions of [1] should be more applicable. The spectrometer was therefore re-configured so that one of the analysers was positioned in a forward direction $\theta_a = 35^\circ$, while the other was rotated around the detection plane. The fixed analyser was set to collect electrons at an energy of 80 eV while the second analyser detected electrons of 5 eV. The momentum transfer vector $\mathbf{q} = \mathbf{k_i} - \mathbf{k_a}$ was therefore at an angle of 62° to the forward direction.

Results were obtained between $\theta_b = 35^\circ$ and $\theta_b = 125^\circ$ to establish the forward binary structure in the cross section using the same arrangement as detailed above. To obtain results in the recoil $-\mathbf{q}$ direction, the electron gun was rotated to the perpendicular plane geometry, allowing the second analyser to pass through $\theta_b = 180^\circ$ and move to the same side as the fixed analyser. The electron gun was then rotated back to the coplanar geometry and the coincidence experiment once more commenced. The second analyser was limited between $\theta_b = 237.5^\circ$ and $\theta_b = 287.5^\circ$ again by the position of the electron gun and the fixed analyser.

Figure 6 shows the results from these experiments, once more normalized to unity at $\theta_b = 45^\circ$. The direction of $\pm\mathbf{q}$ is also shown for reference. The structure seen in the $+\mathbf{q}$ direction peaks at an angle $\theta_b \sim 68^\circ$, which is slightly larger than that of the momentum transfer direction. This forward 'binary' peak is a well-defined structure which is also seen in asymmetric ionization studies from atomic targets, and is thought to be due to the direct collision between the incident electron and one of the valence electrons. The results taken in the $-\mathbf{q}$ direction are small and largely featureless, indicating that within the measured angular range of the spectrometer, the backscatter structure is uniform. This 'recoil' structure is usually attributed to a binary collision followed by elastic scattering of the slow electron from the ionic core [28].

The results presented here compare reasonably with earlier results by Ehrhardt and co-workers [28] who studied ionization of H_2 in a coplanar asymmetric geometry. The nearest results in their study were for $E_{inc} = 100$ eV, $E_a = 4.5$ eV and $\theta_a = 25^\circ$, where they found a binary peak at $\theta_b = 78^\circ$ with a peak width of 80°. They could not detect a recoil peak under their operating conditions. By contrast, for the results presented in this paper, $E_{inc} \sim 100.3$ eV, $E_a = 5$ eV and $\theta_a = 35^\circ$, with the binary peak at $\theta_b = 68^\circ$ having a peak width of 50°. The ratio for the binary to recoil peak cross section is measured to be ~7:1.

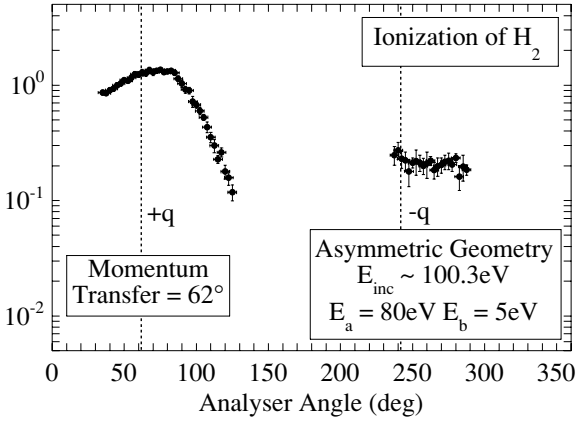

Figure 6. Experimental results for ionization of H_2 in a coplanar asymmetric geometry for an electron of energy 80 eV forward scattered at an angle $\theta_a = 35^\circ$. The low energy electron of energy 5 eV is detected as a function of the angle θ_b. The angle of the momentum transfer vector $\mathbf{q} = \mathbf{k_i} - \mathbf{k_a}$ is also shown.

4. Comparison with theory

One of the aims of these studies was to ascertain whether Young's double-slit-type interference is observed from H_2 due to the distributed scattering centres presented by the nuclei in the molecule. The differences between H_2 and He observed here *may* indicate that this type of interference is occurring; however no current low energy theory exists with which to compare these results. Stia and colleagues [1] have presented a theoretical analysis for an asymmetric geometry at high incident energy. The essential features of their analysis indicate that the molecular DCS is given by an oscillating factor which modulates the cross section for ionization of a hydrogen atom. Their analysis used a simple volume integration to average the cross section over all directions of the inter-nuclear axis (i.e. for ionization from H_2 randomly oriented in space, as in these experiments). The predicted cross section is then given by

$$\mathrm{DCS}^{\mathrm{Aver}}_{\mathrm{H_2}} \cong 2\left[1 + \frac{\sin(|\chi||\mathbf{R}|)}{|\chi||\mathbf{R}|}\right]\sigma_{\mathrm{H}} = M(E_{\mathrm{inc}}, \theta_a, \theta_{\mathrm{b}})\sigma_{\mathrm{H}} \tag{9}$$

where σ_{H} is the ionization cross section from atomic hydrogen, $\mathbf{R}$ is a vector along the inter-molecular axis, and $\chi = \mathbf{k_a} + \mathbf{k_b} - \mathbf{k_i}$ where $\mathbf{k_i}, \mathbf{k_a}, \mathbf{k_b}$ are the momenta of the incident and scattered electrons (see figure 1).

Equation (9) is derived from a high energy model assuming asymmetric energies and angles, and which ignores exchange. Since no models yet exist for low energy ionization of H_2, this expression is modified here to include both symmetric and asymmetric geometries, recognizing that the comparison between experiment and theory is likely to be poor.

Choosing the z-axis along $\mathbf{k_i}$, for a coplanar symmetric geometry $|\mathbf{k_a}| = |\mathbf{k_b}|$ and $\theta_{\mathrm{a}} = \theta_{\mathrm{b}} = \theta$. In this case equation (9) reduces to

$$\mathrm{DCS}^{\mathrm{Aver}}_{\mathrm{H_2}} \cong 2\left[1 + \frac{\sin(R(2|\mathbf{k_a}|\cos\theta - |\mathbf{k_i}|))}{R(2|\mathbf{k_a}|\cos\theta - |\mathbf{k_i}|)}\right]\sigma_{\mathrm{H}} = M(E_{\mathrm{inc}}, \theta)\sigma_{\mathrm{H}} \tag{10}$$

where $R = 0.742$ Å $= 1.406$ au and $\mathbf{k_i}, \mathbf{k_a}, \mathbf{k_b}$ are in atomic units. The modulation function $M(E_{\mathrm{inc}}, \theta)$ has been calculated at the energies used in these experiments, and is shown in figure 7.

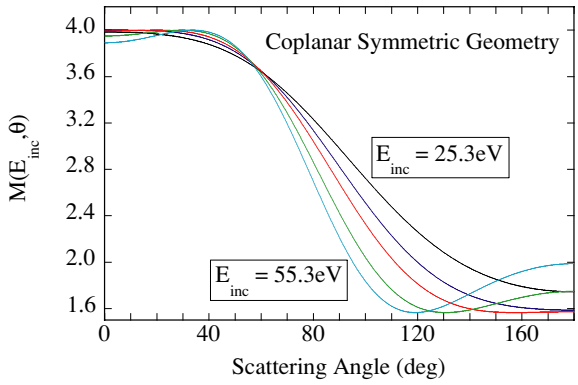

Figure 7. Calculated modulation function $M(E_{\rm inc}, \theta)$ for a coplanar symmetric geometry based upon the theoretical work of [1], for the experimental energies shown in figure 4. For details, see text.

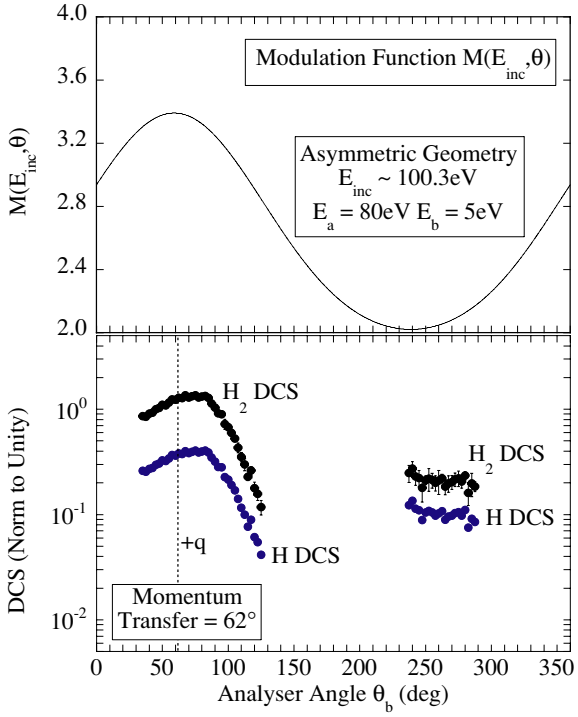

Figure 8. Calculated modulation function $M(E_{\rm inc}, \theta)$ for the coplanar asymmetric geometry based upon the theoretical work of [1], for the experimental results shown in figure 6. The atomic hydrogen differential cross section derived from this function is compared to the measured H_2 cross section.

By rearranging equation (10), the cross section for ionization of atomic hydrogen can be predicted. Although no experimental results exist for ionization of H at low energies in a coplanar symmetric geometry, it is expected that the DCS will be similar to that of helium and other atomic targets, with a peak at $\theta \sim 45^\circ$, a minimum around $\theta \sim 75^\circ$ and a peak in the

backward direction at $\theta \sim 125^\circ$. Assuming this structure also applies to H, it is immediately obvious from figure 6 that the modulation function $M(E_{\rm inc}, \theta)$ *cannot* produce the new feature at $\theta \sim 75^\circ$ observed in H_2. Within the constraints of this model, the features observed in H_2 are therefore not expected to be due to Young's double-slit-type interference. A full low energy multiple scattering centre theory such as recently derived for N_2 [2] is clearly needed to elucidate the origin of these structures.

By contrast, equation (9) should be directly applicable to the asymmetric results presented in figure 6. The modulation factor for these operating conditions is shown in figure 8, together with the predicted atomic hydrogen DCS under these conditions. Once again the modulation function does not indicate whether Young's type interference is occurring, as the predicted atomic cross section is not unusual. No experimental results are available with which to compare this predicted cross section, so again it is not possible to comprehensively ascertain the importance of this type of interference to the overall cross section.

5. Conclusions

Coplanar symmetric and asymmetric results have been presented for ionization of H_2 in the low to intermediate energy regime. Results from a coplanar symmetric geometry reveal an unusual feature in the cross section around $\theta \sim 75^\circ$ which is not seen in atomic targets, nor in ionization from N_2 at similar energies. It is suggested that this feature comes from the charge distribution around the double scattering centres provided by the two nuclei in the H_2 molecule. Results for asymmetric scattering at 100.3 eV incident energy show the usual binary and recoil peaks expected in this geometry, with an absence of any signature from the feature at $\theta \sim 75^\circ$ observed in a symmetric geometry. It is therefore considered that the coplanar symmetric geometry provides a more sensitive test of the effects of the double scattering mechanism in H_2.

The experimental setup does not measure the direction of the molecular axis during the collision, and so averages over all possible orientations of the target. The vibrational state of the neutral target is $v = 0$; however due to the Franck–Condon overlap, vibrational states from $v' = 0$ to 6 are excited in the ground state of the H_2^+ ion during the collision. Since the orientation of the molecule is not determined in the experiment, the rotational states of the molecule excited during the collision will not play a significant role.

One of the reasons for studying H_2 was to determine whether the effects of Young's double-slit-type interference from the two scattering centres in the hydrogen molecule could be observed in the ionization process. This effect has been predicted for diatomic targets at high incident energies in an asymmetric geometry, however no low energy measurements have been conducted until now. Based upon these high energy models, there is little evidence in the experimental results presented here of this type of phenomenon occurring. There are however, significant differences between ionization from H_2 compared to atomic targets which must be due to the distributed charges in the molecule. Whether these are due to Young's type interference, or perhaps are due to the more conventional interference terms which give rise to the structure in all ionization differential cross sections, remains to be seen. This question can only be answered when a full low energy model of the ionization process is forthcoming.

Acknowledgments

The Engineering and Physical Sciences Research Council (EPSRC) is thanked for supporting this work. Mr Alan Venables and Mr Dave Coleman are also thanked for providing continual

technical support for the (e, 2e) spectrometer, and for modifying the apparatus for use with hydrogen.

References

[1] Stia C R, Fojón O A, Weck P F, Hanssen J and Rivarola R D 2003 *J. Phys. B: At. Mol. Opt. Phys.* **36** L264
[2] Gao J, Madison D H and Peacher J L 2004 Private communication
[3] Cohen H D and Fano U 1966 *Phys. Rev.* **150** 30
[4] Martin J 1966 *J. Phys. B: At. Mol. Opt. Phys.* **32** R197
[5] Stolterfohrt N *et al* 2001 *Phys. Rev. Lett.* **87** 023201
[6] Stolterfohrt N, Sulik B, Gulyás L, Skogvall B, Chesnel J Y, Frémont F, Hennecart D, Adoui L, Husson Hossain S and Tanis J A 2003 *Phys. Rev.* A **67** 030702
[7] Misra D, Kadhane U, Singh Y P, Tribedi L C, Fainstein P D and Richard P 2004 *Phys. Rev. Lett.* **92** 153201
[8] Takahashi M, Watanabe N, Khajuria Y, Udagawa Y and Eland J H D 2004 *Book of Contributed Papers, Int. Conf. on Electron and Photon Impact Ionization and Related Topics (Louvain-la-Neuve, 1–3 July)*
[9] Murray A J, Turton B C H and Read F H 1992 *Rev. Sci. Instrum.* **63** 3346
[10] Lohmann B 2004 Private communication
[11] Bransden B H and Joachain C J 2003 *Physics of Atoms and Molecules* (Harlow: Prentice-Hall)
[12] Hussey M J and Murray A J 2002 *J. Phys. B: At. Mol. Opt. Phys.* **35** 3399
[13] Rioual S, Vien G N and Pochat A 1996 *Phys. Rev.* A **54** 4968
[14] Murray A J and Read F H 1992 *Phys. Rev. Lett.* **69** 2912
[15] Murray A J and Read F H 1993 *Phys. Rev.* A **47** 3724
[16] Murray A J, Woolf M B J and Read F H 1992 *J. Phys. B: At. Mol. Opt. Phys.* **25** 3021
[17] Bowring N J, Murray A J and Read F H 1999 *J. Phys. B: At. Mol. Opt. Phys.* **32** L57
[18] Murray A J, Bowring N J and Read F H 2000 *J. Phys. B: At. Mol. Opt. Phys.* **33** 2859
[19] Murray A J and Read F H 2000 *J. Phys. B: At. Mol. Opt. Phys.* **33** L297
[20] Murray A J and Cvejanovic D 2003 *J. Phys. B: At. Mol. Opt. Phys.* **36** 4875
[21] Murray A J 2005 *Phys. Rev. Lett.* in preparation
[22] Hussey M J and Murray A J 2005 *J. Phys. B: At. Mol. Opt. Phys.* in preparation
[23] Nelder J A and Mead R A 1965 *J. Comput.* **7** 308
[24] Varian Inc., www.varianinc.com
[25] Brunt J N H, King G C and Read F H 1977 *J. Phys. B: At. Mol. Phys.* **10** 1289
[26] Comer J and Read F H 1971 *J. Phys. B: At. Mol. Phys.* **4** 368
[27] Bowring N J, Murray A J and Read F H 1997 *J. Phys. B: At. Mol. Opt. Phys.* **30** L671
[28] Jung K, Schubert E, Paul D A L and Ehrhardt H 1972 *J. Phys. B: At. Mol. Phys.* **8** 1330